Appl. Phys. B 71, 573–580 (2000) / Digital Object Identifier (DOI) 10.1007/s003400000375

Applied Physics B
Lasers
and Optics

Remote sensing of the atmosphere using ultrashort laser pulses

P. Rairoux[3,*], H. Schillinger[2], S. Niedermeier[2], M. Rodriguez[1], F. Ronneberger[2], R. Sauerbrey[2], B. Stein[1], D. Waite[1], C. Wedekind[1], H. Wille[1], L. Wöste[1], C. Ziener[2]

[1] Freie Universität Berlin, Institut für Experimentalphysik, Arnimallee 14, 14195 Berlin, Germany
(Fax: +49-30/8385-5665, E-mail: holger.wille@physik.fu-berlin.de)
[2] Friedrich-Schiller-Universität Jena, Institut für Optik und Quantenelektonik, Max-Wien-Platz 1, 07743 Jena, Germany
(Fax: +49-3641/947-202, E-mail: sauerbrey@qe.physik.uni-jena.de)
[3] Alfred-Wegener-Institute for Polar and Marine Research, Telegrafenberg A43, 14473 Potsdam, Germany

Received: 8 December 1999/Revised version: 18 May 2000/Published online: 16 August 2000 –

Abstract. Theoretical and experimental studies were performed on the propagation of ultrashort optical terawatt pulses through the atmosphere. Propagation simulations of intense sub-picosecond pulses show that non-linear processes, such as white light generation, can be initiated at a chosen distance by selecting an appropriate group velocity dispersion. With this technique, a white light continuum was generated in the atmosphere whose spectral distribution was characterised in the visible and near infra-red. Applications of this novel light source for atmospheric remote sensing were investigated, combining lidar and time-resolved broadband absorption spectroscopy techniques. Measurements were performed on the oxygen molecule and water vapour. A comparison between the experimental results and the tabulated spectroscopic data led to an excellent correlation with measurements made on water vapour whereas observations on the oxygen showed discrepancy. This study demonstrates that the remote generation of a white light source represents a new way to access the range-resolved multi-trace gas analysis in the atmosphere.

PACS: 42.68.-wt; 42.62.Fi; 42.65.Re

During the past decade, atmospheric monitoring using optical remote sensing techniques has led to an improved comprehension of physical and chemical processes in the atmosphere. The lidar technique (light detection and ranging) [1], as a range-resolved method applying a pulsed laser as light source, has shown its ability to monitor trace gases and aerosols from the ground level up to the stratosphere with a high range resolution [2–7]. Long-path absorption methods as range integrated methods, such as DOAS (differential optical absorption spectrometer) in the UV and visible spectral range [8–10] and FTIR (Fourier transform infra-red spectrometer) in the infra-red spectral region [11], allow a multi-trace gas analysis, using the sun, moon or a spectral lamp as light source. Despite these improvements, a simultaneous and range-resolved characterisation of the chemical and physical behaviour of atmospheric processes is required. This concerns not only trace gases [12, 13], but also atmospheric aerosols [14, 15].

The novel atmospheric monitoring method presented in this paper makes a contribution to fulfilling this requirement. This technique is based on the application of time-resolved absorption spectroscopy to a pulsed broadband light source in order to perform range-resolved multi-trace analyses simultaneously [16, 17]. The novel element in this method is the light source, which is a white light continuum or supercontinuum (SC). It is generated in the atmosphere using high peak-power laser pulses with pulse duration in the fs time-domain.

In the field of remote sensing, several studies have been performed using ultrashort laser pulses. It has been demonstrated that chirp laser pulses can be applied to elaborate a high-resolution range finder [18]. Precursory laboratory work [19, 20] has reported that by probing liquid aerosol with fs pulses, the third harmonic can be generated by the particles, which can be applied to sizing the aerosols. We have previously demonstrated [21] that a SC can be generated in the atmosphere using intense fs pre-chirped laser pulses. The broadband light emission was spectrally characterised between 450 nm and 850 nm. Observation of the white light continuum propagation through the atmosphere up to an altitude of 12 km confirmed that the SC emission is not diffused but has laser-like beam characteristics and also remains collimated along its propagation path through the atmosphere.

The generation of a SC in gases with ultrashort pulses operating in the gigawatt regime is a well-observed phenomenon [22, 23]. In recent experiments [24], applying the state-of-the-art terawatt fs lasers, the production of intense white light in air and the generation of stabilised light filaments by the focused laser pulses have been observed. Those filaments propagate over distances of ten metres or more and together they form a bundle called a channel. Two scenarios could actually explain this phenomenon: one is based on the model of moving focus [25] and the other is related to the balance between self-focusing, ionisation and diffrac-

[*] *Present adress:* Brandenburgische Technische Universität Cottbus, Luftchemie, Max Planck Str. 11, 12489 Berlin, Germany
(Fax: +49-30/6392-5654, E-mail: rairoux@btu-lc.fta-berlin.de)

tion [26, 27]. Observation of free charges in the channel recently reported by Schillinger et al. [28] would support the second explanation. A possible explanation of the SC formation in normal dispersive media was proposed by several authors [29, 30]. They studied the changes in pulse shape in the presence of a non-linear modification of the group velocity dispersion (GVD). It was numerically and experimentally found [31] that fs pulses split into several shorter sub-pulses. This not only provides a mechanism to hinder catastrophic self-focusing (by limiting the peak intensity), but additionally, self-phase modulation of the sub-pulses leads to a very strong spectral broadening.

1 Propagation of high-intensity optical pulses

The propagation of short and intense laser pulses in the terawatt regime through the atmosphere is different from the well-known and largely used nanosecond pulses [1, 32]. Propagation effects due to the large spectral bandwidth of ultra-short pulses (group velocity dispersion), the non-linear effects related to the sub-ps time scale and the high intensity have to be considered. Self-focusing and other non-linear processes such as filament creation and SC generation occur (see Fig. 3) when pulse intensity exceeds the 10^{10} W/cm^2 [24, 25] threshold. Moreover, increase in the intensity above 10^{13} W/cm^2 leads to a plasma formation.

To yield high intensities and to generate a white light continuum at selected distance away from the laser source, the group velocity dispersion (GVD) change should be compensated and the phase front distortion should be considered. The group velocity dispersion describes the temporal (and spectral) spread of a laser pulse when it propagates through a dispersive medium. For fs pulses and propagation lengths through air of the order of hundreds of metres, the laser peak power may thus be affected by orders of magnitude. To the lowest order, GVD causes a quadratic change in phase of the light pulse, equivalent to a linear change in frequency along the co-propagated reference frame. Such a linear chirp is usually included in the field amplitude function of the laser pulse by a parameter β. This parameter, and consequently the temporal intensity of the pulses, changes linearly with path length far away from the shortest pulse duration. With $\Delta t_{\min}$ denoting the shortest pulse duration, the pulse length F that changes along the path is:

$$F(x, \nu, \Delta t_{\min}) = \Delta t_{\min} \sqrt{1 + \frac{4 \ln(2) \beta(x, \nu)^2}{\Delta t^2{}_{\min}}}, \qquad (1)$$

where $\beta(x, \nu)$ is the GVD at frequency centre ν after the path-length x. For a pulse with a Gaussian pulse shape, this is in perfect analogy with the variation of the beam waist of a Gaussian beam along its light path. The dispersive property of the optical medium enters into β via the second derivative of the refractive index n with respect to frequency:

$$\beta(x, \nu) = \frac{x\nu}{2\pi c} \frac{\partial^2}{\partial \nu^2} n(\nu)\,. \qquad (2)$$

Only for very short pulses and strongly dispersive media such as liquids would one have to include higher chirp contributions (quadratic and cubic chirp, corresponding to cubic and quadratic phase terms). However, this is not considered in this study. Figure 1a shows simulation of pulse shortening effect using (1) and (2), assuming that the laser pulse is launched vertically into the atmosphere. In this case, we compute the second derivative of the refractive index from its dispersion according to the literature [33]. The altitude temperature dependence of the refractive index was considered using a standard atmosphere [33]. Three different final pulse durations at 5 km altitude were considered, 60, 120 and 240 fs, respectively. The initial pulse duration at the position of the laser

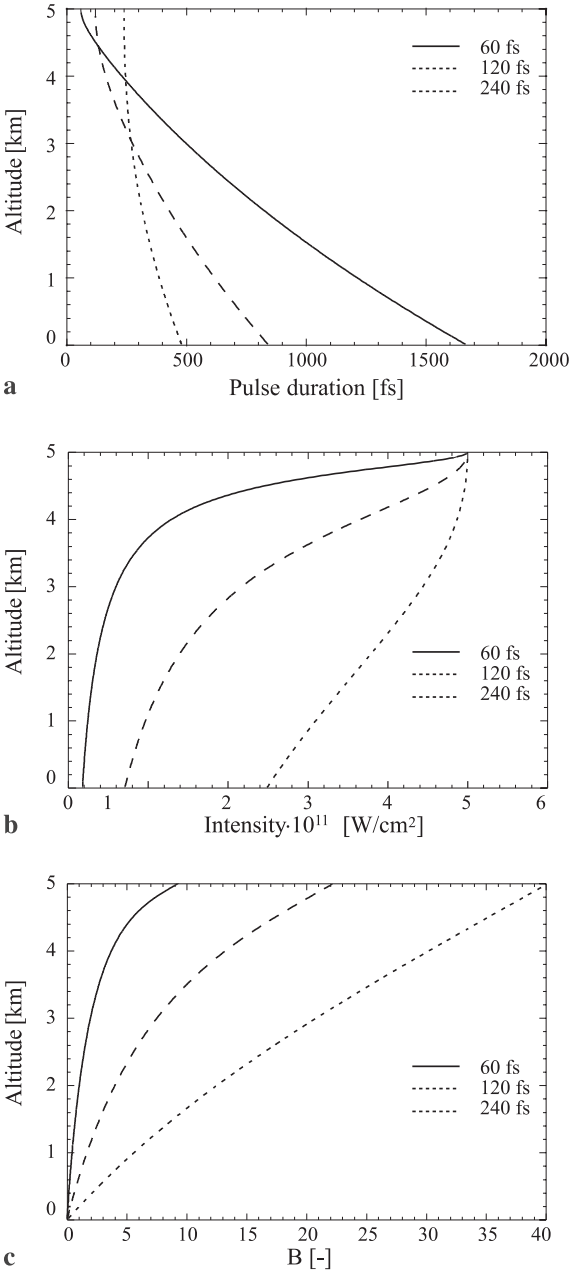

Fig. 1a–c. Simulation of intense laser pulse transmission through the atmosphere. Three pulse durations were considered (*full line*: 60 fs, *dashed line*: 120 fs, *dotted line*: 240 fs). **a** Pulse duration shortening with path-length due to the group velocity dispersion change. **b** Pulse intensity increase with altitude, using the pulse duration change shown in **a**. **c** Variation of the *B*-integral with the path-length. The vertical distribution of the pulse intensity, shown in **b**, is taken in consideration

source was retrieved by backward computation. Hence, this simulation shows that it is possible to launch a short pulse with an appropriate negative pre-chirp and initial pulse duration, in such a way that it is compressed to its minimum pulse length after travelling the desired distance. As arranged in the experimental setup (Fig. 2), in chirped pulse amplification (CPA) laser systems the initial amount of linear chirp can easily be aligned via the distance of the optical compressor gratings.

The advantage of this pre-chirping technique is that the achievement of the desired intensity to initiate non-linear effects, such as self-focusing and continuum generation at a position distant from the laser source, does not require the launch of an intense pulse. This is well shown in Fig. 1b. To generate a field intensity of $5 \times 10^{11}\,\mathrm{W\,cm^{-2}}$ at 5 km altitude, an initial pulse intensity of less than a tenth of the final intensity is required, provided that the pulse is adequately pre-chirped.

When the fs pulse is propagating through the atmosphere, a wave-front distortion is induced. To estimate this effect, the B-integral is introduced as the widely accepted measure:

$$B = \int \frac{2\pi}{\lambda} n_2 I(x)\,\mathrm{d}x, \tag{3}$$

where λ is the emitted wavelength, n_2 the non-linear refractive index and $I(x)$ the pulse intensity at distance x (for air, $n_2 = 5.6 \times 10^{-19}\,\mathrm{cm^{-2}\,W^{-2}}$ [34]). Computation of the path-length dependence of this integral is presented in Fig. 1c. Three pulses with the same 100 GW peak power and different pulse durations (60, 120 and 240 fs) were evaluated. A surface area of $1200\,\mathrm{cm^2}$ (40 cm diameter) for the sending optics was assumed. The results in Fig. 1c show that the shortest pulse with the smallest phase front distortion reaches a B value of 9 at an altitude of 5 km. A value for B of less than 10 is required to initiate non-linear processes. With B-values above this threshold, the pulse can be considered as highly distorted and consequently non-linear processes would be annihilated.

As a summary of Fig. 1, application of a convenient laser pulse results in a time focusing in height (small waist, Fig. 1a), in a reduction of non-linear effects at undesired position (lower intensity, Fig. 1b) and in reduced pulse front distortions (smaller B-integral, Fig. 1c).

2 Experimental

The set-up of the broadband white light lidar experiment is displayed in Fig. 2. On the emitter side, it consists of a table-top terawatt fs laser system, a pulse compressor and a beam steering optics. The laser system is based on titanium-doped sapphire as the amplifying medium and employs CPA technique. The laser operates at 790 nm with a maximum output pulse energy of 220 mJ at a repetition rate of 10 Hz. The final pulse duration is adjustable according to the distance between the compressor gratings and amounts to 100 fs (FWHM) at optimum alignment. The pulse duration was measured with different second and third autocorrelators and frequency-resolved optical gating (FROG) techniques. The spectral width of the pulse was 11 nm. Longer pulse durations with a linear change of wavelength in time, a so-called

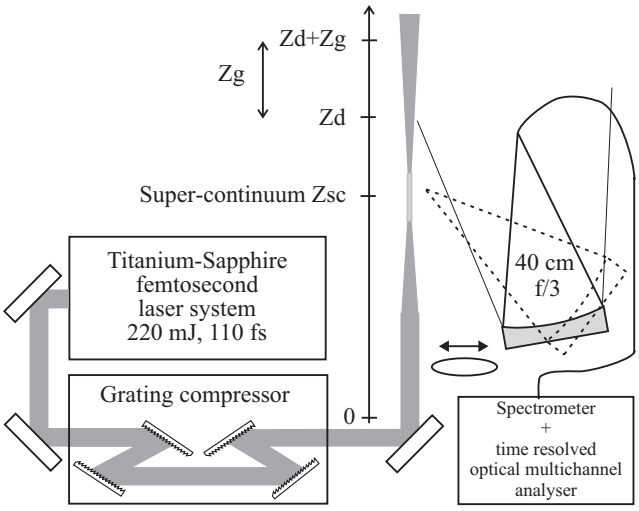

Fig. 2. Experimental set-up of the broadband white light lidar. The geometry of the light detection is presented along the laser beam where z_{sc} is the altitude of the SC generation, z_d the altitude of signal recording using the gated OMA and adjustable, z_g the distance on which the signal is averaged by the OMA

positive or negative linear chirp, have been introduced by the compressor alignment to compensate for the spread of ultrashort pulses by group velocity dispersion in optical media such as lenses or air.

Pulses of 2.2 TW peak power (for optimum compressor alignment) were guided out of the laboratory and sent vertically into the sky. The pulses were either slightly focused with a positive lens ($f = 30$ m), or they were not focused at all.

On the receiver side, the white light continuum backscattered from the atmosphere was collected with a 40-cm-diameter $f/3$ telescope in a bistatic configuration and focused into a 1-mm transmitting fibre bundle. The received light was simultaneously spectrally and temporally resolved using an imaging spectrometer coupled to a time-gated optical multichannel analyser (OMA) (Scientific Instrument), whereby the spectral range of the measurement lay between 250 nm and 850 nm (the cut-off wavelength at 850 nm is related to the quantum efficiency of the S20 photocathode-based OMA-image intensifier). The OMA was based on a diode array with a 30-μm pixel width and a read-out noise of $20\,\mathrm{e^-}$/pixel. The diode signal was converted to digital figures within a 14 bits dynamic range.

The gated OMA detector system recorded and integrated the return signal at an adjustable time delay t_d after the start of the laser pulse which set the range of the measurement z_d. The integration time interval t_g was adjustable from 1.5 μs to 15 μs and it determines the range resolution z_g, which lay between 100 m and 1 km. Regarding the measurement geometry depicted in Fig. 2, the range-resolved signal $N(z_d, \lambda)$ (in units of photon per second) detected within the range interval $(z_d,\ z_d + z_g)$ at the wavelength λ is given by:

$$N(z_d, \lambda) = N_{sc}(z_{sc}, \lambda)\eta(\lambda)A_0 \times \int_{z_d}^{z_d+z_g} \frac{\beta(\lambda, z)}{z^2} \exp\left[-\int_{z_{sc}}^{z} \alpha(\lambda, z^*)\mathrm{d}z^* - \int_{0}^{z} \alpha(\lambda, z^*)\mathrm{d}z^*\right] \mathrm{d}z, \tag{4}$$

where $z_d = ct_d/2$, $z_g = ct_g/2$ (factor of two due to the back and forth propagation of the light), $N_{sc}(z_{sc}, \lambda)$ represents the photon emission rate of the SC generated at the range z_{sc}, $\eta(\lambda)$ the spectral transmission of the receiver, A_0 the telescope surface, $\beta(z, \lambda)$ the volume backscattering coefficient (in unit of $cm^{-1}\,str^{-1}$) at the range z which consists of the molecular Rayleigh part and the aerosol Mie part. The exponential term describes the atmospheric transmission and follows Lambert−Beer's law, where $\alpha(z^*, \lambda)$ is the total volume attenuation coefficient (in unit of cm^{-1}) at the range z^*. This represents the sum of the molecular Rayleigh and aerosols Mie extinction coefficients and the absorption coefficients of the atmospheric traces at the wavelength λ. Equation (4) presents the linear lidar equation [40]. Its application, describing the SC light backscattered from the atmosphere, assumes that the laser emission does not generate other nonlinear processes after the SC generation and that non-elastic scattering like Raman scattering is not detectable by the detector used in the experiment.

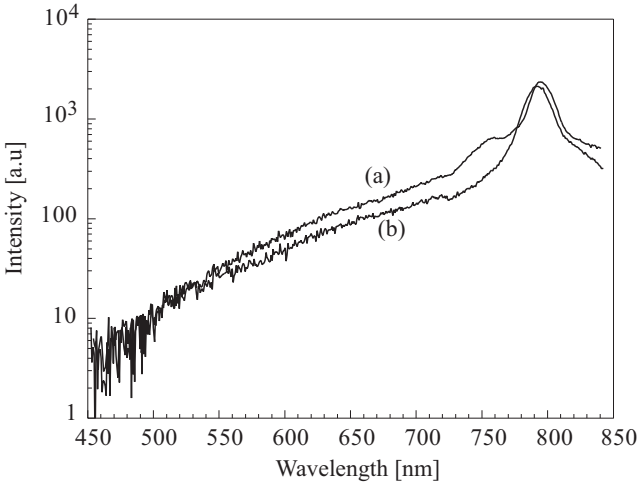

Fig. 3. Spectra of the atmospheric white light continuum. The traces (a) and (b) depict spectra which were measured for two different pre-chirp settings of the fundamental laser emission

3 Atmospheric investigations

In this section, we present experimental results on the SC generation in the atmosphere and on its application for remote sensing of atmospheric compounds. The study was focused on the SC spectral distribution and on its absorption by the atmosphere.

The numerical simulations presented in Sect. 1 have shown that a SC can be generated in the atmosphere at a chosen distance away from the laser source. To characterise this phenomenon, the experiment depicted in Fig. 2 has been set up with a few changes. Behind the sending mirror, the beam was focused with a 30 m positive lens in order to increase the efficiency of the self-focusing and the white light channel formation. Hereby, the SC was generated at just a few ten metres into the atmosphere. This also provided a synoptic control of the SC generation. On the receiver part, the telescope was pointed in the direction of the SC generation area to collect the main part of the light scattered from the channel. The OMA was coupled to a low-resolution 0.25 m imaging spectrometer whereby time-integrated spectroscopy was performed on the SC. Results are shown in Fig. 3; the spectra show a peak at 790 nm with a spectral width (FWHM) of 20 nm which represents the laser emission (broadened by self-phase modulation), whereas the wings on both sides of the peak characterise the SC. The intensity difference between the two curves results from the different initial pre-chirp settings of the laser pulse. Curve (a) describes the best setting, i.e. the largest signal scattered from the SC. The second broadened peak observed at 750 nm in this curve is related to the self-phase modulation process during the SC generation.

To demonstrate the ability of the method presented, we focus our study on the H_2O and O_2 molecules because their concentration and absorption spectra are well known. For this purpose, the laser beam was launched in the atmosphere without using the focusing optics (see Fig. 2). Provided that the laser pulses are adequately pre-chirped, the SC could be generated at an altitude of 150 m. Similar to a standard lidar set-up, the telescope was aligned almost parallel to the beam

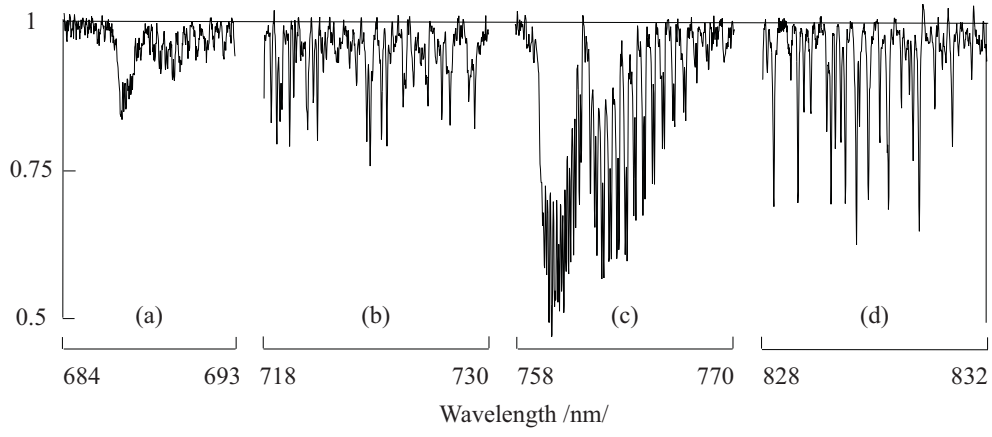

Fig. 4. Range-resolved atmospheric transmission spectra on November 13, 1997 retrieved from the measurements of the SC backscattered from the atmosphere. The delay between each acquired spectrum is 10 min. Different altitudes z_d and different signal-integration ranges were considered for the different spectral intervals (z_d is related to the time delay t_d of the gated detector as described in (4)). Trace (a): $z_d = 550$ m, integration range: 550–1050 m. Trace (b): $z_d = 150$ m, integration range: 150–1050 m. Trace (c): $z_d = 600$ m, integration range: 600–850 m, Trace (d): $z_d = 550$ m, integration range: 550–1100 m

providing a correct overlap between the field of view of the receiving optics and the laser beam. The OMA was coupled to a 0.5-m imaging spectrometer with a spectral resolution of 1 cm^{-1} (60 pm). Time-resolved spectroscopy using the OMA in its gating modus was performed on the SC backscattered from the atmosphere. The efficiency of this method strongly depends on the spectral energy density of the light source and because we performed time-resolved measurements on the SC backscattering, this is more demanding than the previously used time- or range-integrated method. The intensity fluctuations in time of the light source can also limit efficiency, but simultaneous recording of the extended spectral range overcomes this limitation.

The retrieved atmospheric transmission in the 680 – 850 nm spectral range is presented in Fig. 4. Only the spectral regions showing absorption features are presented in this graph. The spectra were recorded at different times due to the limited operating spectral range of the detector (12 nm simultaneously). Moreover, to optimise the signal-to-noise ratio, the spectra were acquired for different altitudes and different integration ranges of the signal. The observed transmission decrease is related to the absorption of the atmospheric constituents on a optical path-length defined by the difference between twice the distance from the ground level to the considered altitude and the SC generation area height (150 m). These observations demonstrate, for the first time, that the amplitude of the SC spectral energy density is high enough to observe range-resolved absorption signatures of atmospheric compounds. In Fig. 4, the two ro-vibrational absorption bands of the O_2 electronic $b^1\Sigma^+_g \leftarrow X^3\Sigma_g$ transition are well characterised: the $v' = 1 \leftarrow v'' = 0$ (spectrum a) and the $v' = 0 \leftarrow v'' = 0$ (spectrum c) in the 684–693 nm and 758–770 nm spectral range, respectively. The spectra (b) and (d) show the signature of the rotational absorption transitions of the H_2O vibrational overtone bands. These spectra are displayed in more detail in Fig. 5a,b. In Fig. 5c a comparison between the measured transmission spectrum and a line-by-line calculation using Hitran [35] spectroscopic data is shown. There, a Voigt function was considered for the absorption line shape. Obviously, the spectrometer does not resolve the narrow transition lines (10 pm) and, as expected, all observed absorption peaks could be attributed to water vapour absorption transitions.

To retrieve the water vapour content in the atmosphere from the measurements, a fit of the calculated absorption spectra was made on the observations using (4). The calculated spectrum was smoothed to the spectrometer resolution after applying Lambert−Beer's law. The water vapour mixing ratio retrieved from the spectra 5a and 5b was 0.6%. This represents a plausible mixing ratio value for the water content into the planetary boundary layer and it agrees with the humidity recorded at ground level with a standard hygrometer. Unfortunately, simultaneously radio-sounding measurements were not accessible to confirm this result. The estimated accuracy of the H_2O mixing ratio is 15% and it is mainly restricted by the determination of the SC generation height which contributes to the absorption path-length (see (4)).

The transmission spectra showing the O_2 absorption transition are depicted in more detail in Fig. 6. The observed difference between the absorption magnitude of the two spectra results from the smaller absorption cross-section of the $v' = 1$ transitions compared to that one of the $v' = 0$ level

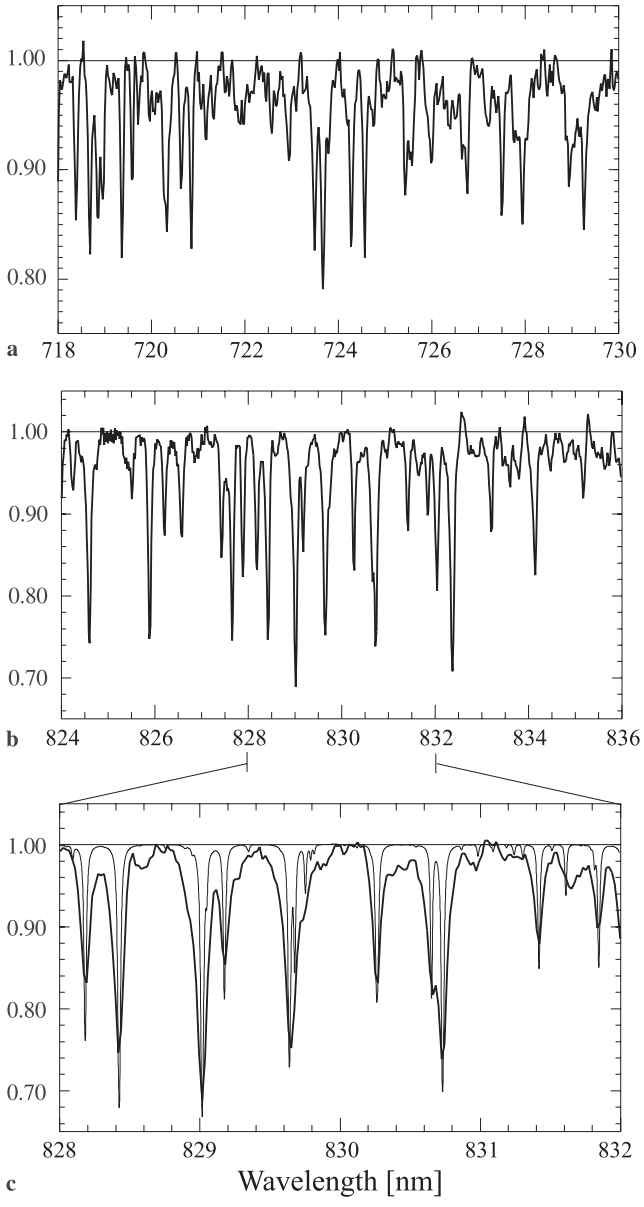

Fig. 5a–c. High-resolution spectra of the range-resolved atmospheric transmission showing the ro-vibrational H_2O absorption transitions. **a** $000 \rightarrow 301$ transitions in the 725 nm band, ($z_d = 150$ m, integration range: 150–1050 mm). **b** $000 \rightarrow 211$ and $000 \rightarrow 310$ transitions in the 830 nm band, ($z_d = 550$ m, integration range: 550–1050 m). **c** Spectral expansion around 830 nm with the line-by-line calculation using the Hitran database *(thin line)*. For more clarity, the amplitudes of the calculated transmission are arbitrary

(at the maximum of the P-branch of the spectrum, $\sigma = 2.9 \times 10^{-24}$ cm^2 for $v' = 1$ transitions and $\sigma = 4 \times 10^{-23}$ cm^2 for $v' = 0$ transitions). The absorption features shown in spectrum (6a) at wavelengths below 687 nm should not be attributed to noise but represent weak H_2O absorption transitions, whereby an absorption of less then 1% can be deduced. This absorption detection limit is related to the low performance of the detector based on a diode array (20% max. QE at 400 nm, 20 e^-/pixel read-out noise, and 14 bits A/D converter dynamics), to the inverse square range dependence of the acquired signal ($1/z^2$) and basically to the low backscattering coefficient of the atmosphere (about 10^{-8} cm^{-1} str^{-1} at

680 nm). This also affects the maximum range of the measurements, which reaches an altitude of 1 km.

O_2 absorption spectra were simulated using the same approach as for H_2O spectra. The comparison between line-by-line calculation and the observations is presented in Fig. 6c and it shows the narrow O_2 absorption lines of $0.1\,\mathrm{cm}^{-1}$ which are not completely resolved by the measurements. The weak transitions between the line-doublets can not be easily identified. They could characterise the minor $^{16}O^{18}O$ isotope or non-tabulated atmospheric compounds in this spectral range.

To evaluate the atmospheric O_2 mixing ratio, the previously outlined fit procedure was applied to the measured transmission spectrum presented in Fig. 6b. The result leads to a strong discrepancy: fitting the large transitions (transmission < 0.8), a mixing ratio of 13% could be retrieved, whereas a 21% mixing ratio could be deduced applying the same procedure on the weak transitions (transmission > 0.8) as shown in Fig. 7.

The observations rely on a large optical depth (about 60 at the maximum of the absorption band for a path-length of 1200 m) and an incomplete spectral resolution. These physical and experimental conditions could lead to a classical interpretation of the observed deviation of Lambert−Beer's absorption law where the saturation of the absorption lines can be the apparent reason [36]. The calculation of the light intensity saturation I_s at the maximum of the O_2 absorption band using the classical model [38, 39], shows that the value reaches $4 \times 10^{13}\,\mathrm{W/cm^2}$ which is even higher than the $10^{11}\,\mathrm{W/cm^2}$ intensity of the fundamental laser emission. ($I_s = h\nu/2\sigma\tau$, where ν is the frequency, σ the absorption cross-section at ν, and τ the lifetime of the excited state [39].) An inappropriate concentration evaluation procedure is also not the cause of this discrepancy. To be tested, the fit-procedure was applied to measurements performed in the same spectral region on the sun-light atmospheric transmission using the same experimental arrangement for the detector. Even for strong O_2 transitions, the effective atmospheric optical depth could be correctly deduced [37].

Other aspects of the laser spectroscopy could explain this discrepancy but complementary observations and theoretical investigations are needed to give a reliable explanation: one of them is the transparency phenomenon induced by ultrashort laser pulses propagation in a strong absorbing medium [40]. However, it requires a SC pulse duration shorter than the lifetime of 300 ps of the O_2 excited state [35], which was never observed for SC generation in air. Another phenomenon is the two-photon absorption process [38] which could efficiently arise according to the transition rules of the

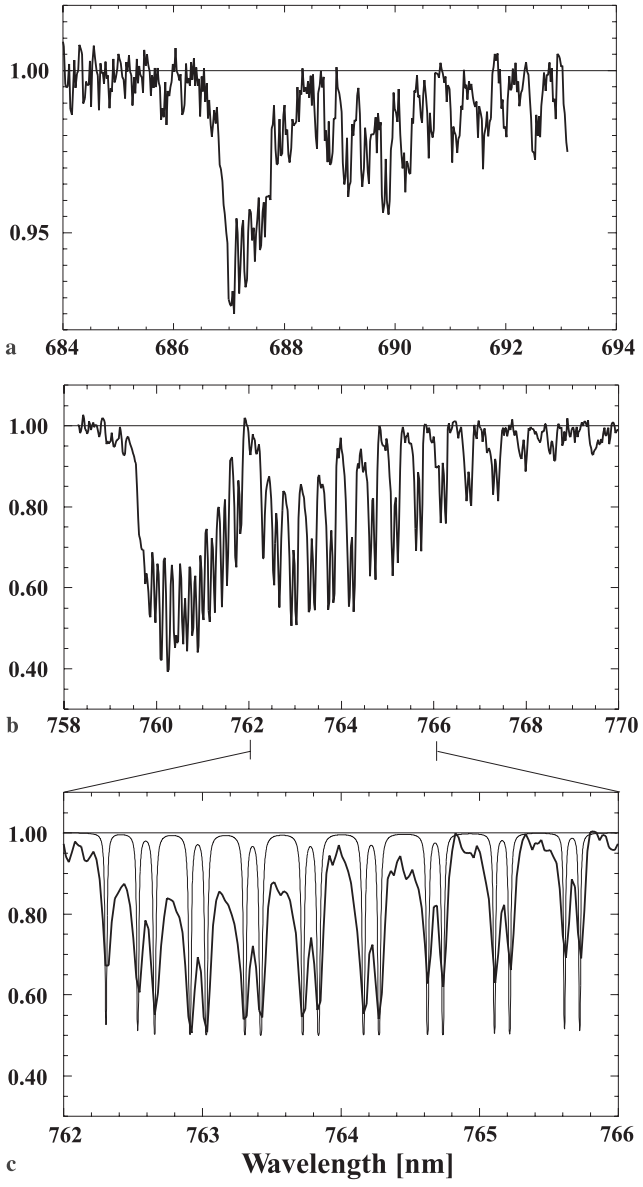

Fig. 6a–c. High-resolution spectra of the range-resolved atmospheric transmission, showing the ro-vibrational molecular Oxygen absorption transitions from the $X\,^3\Sigma_g$ ground state to the excited state $b\,^1\Sigma^+{}_g$. **a** $v''=0 \rightarrow v'=1$ transitions (z_d=550 m, integration range: 550–1050 m). **b** $v''=0 \rightarrow v'=0$ transitions (z_d=600 m, integration range: 600–850 m). **c** Spectral expansion around 764 nm with the line-by-line calculation using the Hitran database *(thin line)*. For more clarity, the amplitudes of the calculated transmission are arbitrary

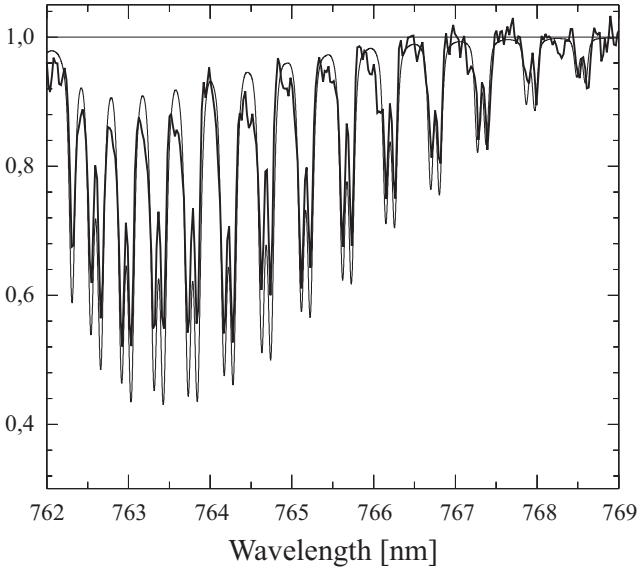

Fig. 7. Comparison between the measured *(full line)* and the fitted *(thin line)* atmospheric transmission spectrum in the O_2 absorption band. A 21% mixing ratio of O_2 was considered to fit the absorption lines. The measurements were ranged at an altitude z_d of 600 m and were integrated between 600 m and 850 m, giving a range resolution of 250 m

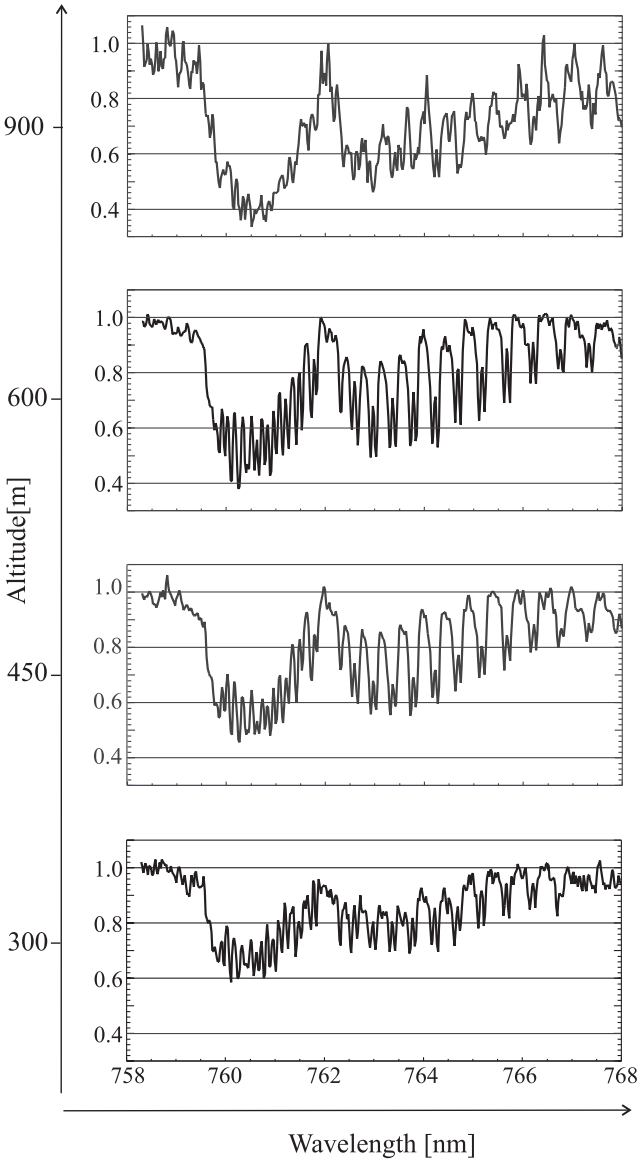

Fig. 8. Vertical profile of the atmospheric transmission spectra in the O_2 absorption band, ranged between 300 and 900 m with a 250 m range resolution. The different altitudes indicated in the figure are given by the time delay t_d of the gated detector (see (4))

$O_2\, b^1\Sigma^+_g \leftarrow X^3\Sigma_g$ transition. Characterisation of the SC in the infra-red spectral region could confirm this fact.

The first demonstration of the ability of this technique to monitor the range-resolved transmission profile of atmosphere is shown in Fig. 8. The spectra relate the atmospheric transmission in the O_2 absorption spectral region between the ground level and the considered altitude. The transmission spectrum obtained for the altitude of 900 m displays a perturbed structure resulting from the degradation of the signal-to-noise ratio.

4 Discussion

In this study, the observations of atmospheric compounds were based on the time-resolved backscattering measurements of the SC propagating through the atmosphere. Because the time resolution t_g of the signal acquisition gives the range resolution of the measurements ($z_g = ct_g/2$), the altitude z_{sc} of the SC generation (see Fig. 2) is not the most significant factor and can be near the ground level. However, the advantage in generating the SC at a higher altitude could be justified by the presence of strong optical absorbers such as thin cloud or haze layers often present in the planetary boundary layer. Hence, the SC generation above such layers would lead to a decrease by a factor of two in their extinction contribution and thus, to an enhancement of the detected signal. If, by using the pre-chirp technique, the intensity of the fundamental emission is high enough to generate a plasma instead of a white light channel at the remote site, the available intensity of the broadband light would hugely increase. Because plasma generation characterises a diffuse light source [41], range-resolved measurements are no longer required and therefore, range-integrated measurements could be made. This will simplify the signal acquisition. Moreover, the vertical profiling could be achieved with the variation of the height of the plasma generation site. This capability should be confirmed by further experiments.

As mentioned in the theoretical part, white light channel or plasma generation is related to a light intensity threshold. This poses an important question: are ultra-short optical pulses really needed to trigger these light source at a remote site or could conventional laser pulses with a ns or ps pulse duration produce the same phenomena? At short distances, they can easily yield non-linear effects or plasma using simple focusing optics, whereas for the generation of the same effects at some hundreds of metres away from the laser source, huge optics are required. This does not even include the wavefront distortion induced by atmospheric turbulence [42]. For example, if we consider a laser with 100 GW peak power at a wavelength of 1 μm, a numerical aperture for the focusing optics of $f/200$ is required to create the 10^{13} W/cm^2 intensity which is necessary to generate non-linear effects and plasma. With a 10-m focal lens, a 50-mm aperture remains realistic, whereas a focal distance of 300 m requires an aperture of more than 150 cm.

Within the detected spectral range (450 to 850 nm), besides H_2O the tropospheric pollutants NO_2 and the nitrate radical (NO_3) could potentially be monitored. Because they play a crucial role in the diurnal ozone chemistry [43], a simultaneous range-resolved monitoring of these three compounds would be important. NO_2 has an absorption band at 450 nm [35], whereas the absorption transitions of NO_3 are found at 623 nm and 662 nm, respectively [44]. In non-polluted atmosphere, NO_2 concentration is in the sub-ppb range and NO_3 level lies between 1 ppt and 150 ppt [43]. Hence, a suitable monitoring of these species requires low-noise measurements with an absorption detection limit in the 10^{-3} range. Because this value reaches 10^{-2} in our observations, that makes it difficult to retrieve these species from the measurements although they lay in the appropriate spectral region. However, it is still possible to retrieve such low absorption levels in this spectral range from lidar measurements when a detector based on a CCD camera is used [16]. Considering this case in combination with the use of the SC as light source, it cannot be excluded that the observed deviation from the Lambert−Beer's absorption law could limit the measurement accuracy of atmospheric trace species.

The spectral distribution observed in the SC (see Fig. 2a) suggests that the SC should have an IR component. This has never been reported in the literature, but the work in progress should confirm this presumption. Because the majority of atmospheric pollutants show absorption features in this spectral region [35, 45], performing remote sensing in IR is attractive, especially for tropospheric purposes in the 3–4 μm spectral interval. There, volatile hydrocarbons such as alkanes and alkenes, which are strongly involved in tropospheric ozone smog formation [13], could be detected [46, 47]. However, the spectral interference between the absorbing compounds and the very low backscattering coefficient of the atmosphere in the IR spectral range (about 10^{-10} cm^{-1} str^{-1}) make these measurements difficult. On the other hand, performing these measurements with the observation method based on the coupling of the lidar with the FTIR technique [17] could overcome these difficulties.

5 Conclusion

The theoretical and experimental studies presented in this paper have shown that non-linear processes such as SC and plasma generated by intense ultrashort laser pulses into the atmosphere could be used for atmospheric remote sensing. Measurements were performed in the visible and near-IR spectral region of the white light channel, using the time-resolved broadband absorption technique coupled to the lidar remote sensing technique. The huge potential of the method could be pointed out as well as its limitation by strong absorption. The application of the SC as a pulsed light source with a spectral extension from UV to IR enables the simultaneous monitoring in a good range resolution of meteorological parameters such as the water vapour content as well as gaseous pollutants. Further studies on plasma generation into the atmosphere and on the extension of the observed spectral band in the UV and IR should confirm and enlarge the capability of this novel atmospheric remote sensing method.

Acknowledgements. The authors gratefully acknowledge H. Haunert from the company Optilas and H. Schlütter from the company Oriel for their technical advice and support for the different OMA detection systems used in this study. Contribution No 1542 Alfred Wegener Institute.

References

1. R.M. Measures: *Laser Remote Sensing* (Wiley, New York, 1984)
2. E.V. Browell, S. Ismail, W.M. Hall, A.S. Moore, S.A. Koii, V.G. Brackett, M.B. Clayton, J.D.W. Barrick, F.J. Schmidlin, N. Scott Higdon, S.H. Melfi, D.N. Whiteman: In Advances in Atmospheric Remote Sensing with Lidar, Selected papers of the 18th ILRC, Berlin 22-26 July 1996 (Berlin, Springer, Heidelberg 1996)
3. M.A. Fenn, E.V. Browell, C.F. Butler: In Advances in Atmospheric Remote Sensing with Lidar, Selected papers of the 18th ILRC, Berlin 22−26 July 1996 (Berlin, Springer, Heidelberg 1996)
4. G. Beyerle, H.-J. Schaefer, O. Schrems, I.S. McDermid: Geophys. Res. Lett. **25**, 919 (1988)
5. B. Stein, M. Del Guasta, J. Kolenda, M. Morandi, P. Rairoux, L. Stefanutti, J.-P. Wolf., L. Wöste: Geophys. Res. Lett **21**, 1311 (1994)
6. C. Wedekind, F. Immler, B. Mielke, P. Rairoux, B. Stein, L. Wöste, M. Del Guasta, M. Morandi, L. Stefanutti, F. Masci, V. Rizi, R. Matthey, V. Mitev, J.-P. Wolf: In Proceedings of the Quadrennial Ozone Symposium L'Aquila, Italy (Library of Congress 1996)
7. D. Weidauer, P. Rairoux, M. Ulbricht: In Advances in Atmospheric Remote Sensing with Lidar, Selected papers of the 18th ILRC, Berlin 22−26 July 1996 (Springer, Berlin, Heidelberg 1996)
8. T. Brauers, M. Hausmann, U. Brandenburger, H.-P- Dorn: Appl. Opt.34, 4472 (1995)
9. U. Platt, D. Perner, H.W. Pätz: J. Geophys. Res **84**, 6329 (1980)
10. D. Perner, A. Roth, T. Klüpfel: Geophys. Res. Lett. **21**, 1367 (1994)
11. J. Notholt, G. Toon, F. Stordal, S. Solberg, N. Schmidbauer, E. Becker, A. Meier, B. Sen: J. Geophys. Res. **102 D11**, 12 855 (1997)
12. D. Kley, P.J. Crutzen, H.G.J. Smit, H. Vömel, S.J. Oltmans, H. Grassl, V. Ramanathan: Science **274**, 230 (1996)
13. National Res. Council: *Rethinking the Ozone Problem* (National Acad. Press, New York 1991)
14. Z. Meng, D. Dabdub, J.H. Seinfelds: Science **277**, 116 (1997)
15. J.H.-F. Heintzenberg, J.H.-F. Graf, R.J. Charlson, P. Warneck: Beitr. Phys. Atmosph. **69**, 261 (1996)
16. I.M. Povey, A.M. South, A. Kint de Roodenbeke, C. Hill, R.A. Freshwater, R.L. Jones: J. Geophys. Res. **103 D3**, 3369 (1988)
17. M. Douard, R. Bacis, P. Rambaldi, A. Roos, J.-P. Wolf, G. Fabre, R. Stringat: Opt. Lett. **20**, 2140 (1995)
18. A. Braun, C.Y. Chien, S. Coe, G. Mourou: Opt. Commun. **105**, 63 (1994)
19. J. Kasparian, B. Krämer, J.P. Dewitz, S. Vadja, P. Rairoux, B. Vezin, V. Boutou, T. Leisner, W. Hübner, J.-P. Wolf, L. Wöste: Phys. Rev. Lett. **78**, 2952 (1997)
20. J. Kasparian, B. Krämer, T. Leisner, P. Rairoux, V. Boutou, V. Vezin, J.-P. Wolf: J. Opt. Soc. Am. B **15**, 1918 (1988)
21. L. Wöste, C. Wedekind, H. Wille, P. Rairoux, B. Stein, S. Nikolov, C. Werner, S. Niedermeier, F. Ronneberger, H. Schillinger, R. Sauerbrey: *Laser and Optoelektronik* (1997)
22. P.B. Corkum, C. Rolland: IEEE J. Quantum Electron. **QE-25**, 2634 (1989)
23. H. Nishioka, W. Odajima, K. Ueda, H. Akuma: Opt. Lett. **20**, 2505 (1995)
24. A. Braun, G. Korn, X. Liu, D. Du, J. Squier, G. Mourou: Opt. Lett. **20**, 73 (1995)
25. A. Brodeur, C.Y. Chien, F.A. Ilkov, S.L. Chin: Opt. Lett. **22**, 304 (1997)
26. F.T.J. Nibbering, P.F. Curley, G. Grillon, B.S. Prade, M.A. Franco, F. Salin, A. Mysyrowicz: Opt. Lett. **21**, 62 (1996)
27. H.R. Lange, G. Grillon, J.-P. Ripoche, M.A. Franco, B. Lamoureux, B.S. Prade, A. Mysyrowicz, F.T.J. Nibbering, A. Chiron: Opt. Lett. **23**, 120 (1998)
28. H. Schillinger, R. Sauerbrey: Appl. Phys. B **68**, 753 (1999)
29. P. Chernev, V. Petrov: Opt. Lett. **17**, 172 (1992)
30. G.G. Luther, J.V. Moloney, A.C. Newell: Opt. Lett. **19**, 862 (1994)
31. J.K. Ranka, R.W. Schirmer A.L. Gaeta: Phys. Rev. Lett. **77**, 3783 (1996)
32. V.E. Zuev, A.A. Zemlyanov, Y.D. Kopytin, A.V. Kuzikovskii: *High-Power Laser Radiation in Atmospheric Aerosols* (Reidel, Dordrecht, Holland 1985)
33. CRCHandbook: *Handbook of Chemistry and Physics*, 69th edn. (CRC Press, Boca Raton, Florida 1988, 1989)
34. Y. Shen: *The Principles of nonlinear Optics*, Vol. 12 (Wiley, New York 1984)
35. L.S. Rothman: The HITRAN molecular database edition of 1991 and 1992. J. Quant. Spectrosc. Radiat. Transfer **48**, 469 (1992)
36. M.W. Sigrist: *Air Monitoring by Spectroscopic* (Wiley, New York 1994)
37. M. Rodriguez: *Diplomarbeit Femtosekunden-Weißlicht-Lidar* (Freien Universität Berlin, Berlin 1998)
38. W. Demtröder: *Laser Spectroscopy Springer Series in Chemical Physics*, Vol. 5 (Springer, Berlin 1988)
39. O. Svelto: *Principles of Lasers* (Plenum Press, New York 1989)
40. M.D. Crisp: Phys. Rev. A **1**, 1604 (1970)
41. G. Bekefi: *Principles of Laser Plasmas* (Wiley, New York 1976)
42. J.W. Strohbehn: *Laser Beam Propagation in the Atmosphere*, Vol. 25 (Springer, Berlin, Heidelberg 1978)
43. U. Platt, D. Perner, J. Schröder, C. Kessler, A. Toennissen: J. Geophys. Res. **86 C12**, 11 965 (1981)
44. A.R. Ravishankara, P.H. Wine: Chem. Phys. Lett **101**, 73 (1983)
45. R.M. Measures: *Laser Remote Chemical Analysis* (Wiley, New York 1988)
46. M.J.T. Milton, T.J. Mc Iveen, D.C. Hanna, P.T. Woods: Opt. Commun. **98**, 186 (1992)
47. R.A. Robinson, P.T. Woods, M.J.T. Milton: Air and Pollution Monitoring, SPIE Proceedings, Munich Fair, Germany **2506**, 140 (1995)